Theoretical shaping of femtosecond laser pulses for molecular photo-dissociation with control techniques based on Ehrenfest's dynamics and time-dependent density-functional theory

Alberto Castro *†

1 Abstract

The combination of the non-adiabatic Ehrenfest-path molecular dynamics (EMD) based on time-dependent density-functional theory (TDDFT), and the quantum optimal control formalism (QOCT) is used to optimize the shape of ultra-short laser pulses in order to achieve the photo-dissociation of the Hydrogen molecule and the trihydrogen cation H_3^+. This work completes a previous one [A. Castro, ChemPhysChem **2013**, 14, 1488-1495], in which the same objective was achieved by demonstrating the combination of QOCT and TDDFT for many-electron systems on *static* nuclear potentials. The optimization model, therefore, did not include the nuclear movement and the dissociation mechanism obtained could only be sequential: fast laser assisted electronic excitation to non-bonding states (during which the nuclei are considered to be static), followed by field-free dissociation. Here, in contrast, the optimization is performed with the QOCT constructed on top of the full dynamical model comprising both electrons and nuclei, as described within EMD based on TDDFT. This is the first numerical demonstration of an optimal control formalism for a hybrid quantum-classical model, i.e. a molecular dynamics method.

2 Introduction

The manipulation of physical processes at the quantum level is generically called "quantum control" [1, 2, 3], an emerging field of Science that is making fast progress both experimentally and theoretically. One of its most impressive suc-

*ARAID Foundation – Institute for Biocomputation and Physics of Complex Systems (BIFI), University of Zaragoza, Mariano Esquillor s/n, Edificio I+D, 50018 Zaragoza (Spain)

†Zaragoza Scientific Center for Advanced Modeling (ZCAM), Mariano Esquillor s/n, Edificio I+D, 50018 Zaragoza, Spain

cess stories is its application for selective photo-chemistry: the shaping of femtosecond laser pulses to induce photo-chemical reactions in molecules [4, 5, 6].

Experimentally, numerous groups are pursuing this objective, typically basing their work on the "adaptive feedback control" experimental setup [7], which uses the fundamental tool needed for this purpose – the laser shaper [8]. Theoretically, the prediction of pulse shapes capable of breaking or creating bonds at will is a challenging task, and is usually attempted with the aid of "optimal control theory" (OCT), the mathematical discipline that is concerned with the optimization of dynamic systems in general [9]. The quantum branch of OCT (QOCT) was born in the 80s, and has quickly developed ever since. In order to be useful, QOCT must be applied on a suitable model for the system and process whose optimization is attempted.

The choice of the model to simulate the dynamical process (the laser-molecule irradiation, in this case) has obvious consequences on the numerical difficulty of the optimization, and on the reliability of the results. Most applications of QOCT in this area have relied on wave packet propagation techniques: they have addressed the motion of nuclear wave packets, on one or a few potential energy surfaces. This may be a very precise model, provided a sufficient number of surfaces is included, and their non-adiabatic couplings are correctly computed. However, the computational cost of pre-computing the surfaces, in addition to the cost of the propagation of the nuclear wave packets, is very high.

A cost reduction may be obtained by taking the classical approximation for the nuclei i.e. using a mixed quantum-classical model. This may be sufficient for many problems, and is the fundamental principle of Molecular Dynamics (MD). There are a large number of MD variants; for the problem of laser-assisted photo-chemistry, we must choose an ab initio formulation capable of dealing with changing bonds, external fields, non-adiabatic electronic transitions and strongly excited electronic systems. This is of course the worst-case scenario for MD models - specially since, on top of it, one must build an OCT formalism (not just the standard quantum or classical one, but one capable of dealing with mixed quantum and classical degrees of freedom together).

One simple alternative is Ehrenfest molecular dynamics (EMD) based on time-dependent density-functional theory (TDDFT) [10, 11]. EMD deals with the issue of mixing quantum and classical degrees of freedom in a straightforward manner, and although suffers from serious shortcomings, provides an acceptable first-order approximation to the solution. TDDFT, on the other hand, is in principle an exact reformulation of the many-electron quantum dynamics problem - yet this formal exactness cannot be realized in practice due to the need of approximating some of its ingredients in the current state of affaires. Finally, the combination of these two techniques (EMD-TDDFT) has been successfully employed in various works in the past[12, 13, 14, 15, 16, 17, 18].

Once the equations of motion that model the physical process have been chosen, the OCT formalism must be constructed. The combination of QOCT with TDDFT was presented in Ref. [19], that also displayed the first numerical results for a simple two-dimensional electronic problem. This theoretical scheme and the corresponding implementation, however, only addressed a purely quantum

(electronic) system.

The combined use of EMD and TDDFT within QOCT was first approached in Ref. [20]. However, the optimization was performed with a gradient-free algorithm that did not use of the main theoretical result provided by OCT: the expression of the gradient of the magnitude that is to be maximized, as a function of the parameters that define the controlling function (a laser pulse, in our case). We did not have, at that time, the complete theoretical OCT framework for a mixed quantum-classical system.

Later, Ref. [21] reported the optimal shaping of laser pulses for molecular photo-dissociation, by making use of the QOCT-TDDFT combination presented in Ref. [19], *even if the movement of classical nuclei was ignored*. This was possible because a truly ultra-fast situation was assumed: the action of the laser pulse was very short, giving no time for the nuclei to react until it was over. The dissociation mechanism could therefore only be sequential: fast laser assisted electronic excitation to non-bonding states (during which the nuclei are static), followed by field-free dissociation. The role of QOCT-TDDFT was then to prepare the electronic system into those non-bonding states, considering fixed nuclei.

This procedure cannot however be employed in general, as it was demonstrated in the very same Ref. [21]: as soon as the laser pulses become long enough, the nuclear movement must be taken into account into the optimization algorithm. Therefore, the OCT formalism for mixed-quantum classical systems in general, and for the EMD-TDDFT model in particular, was needed. This theory was presented in Ref. [22]. This article can be considered the completion of Ref [21], since it solves the limitations reported in that article by making use of the new quantum-classical OCT. It reports the implementation of this theory into the octopus code [23, 24], and a few numerical examples demonstrating its feasibility.

3 Theory and computational aspects

The main results of the theory presented in Ref [22] will be summarized here, as well as the key aspects of the corresponding numerical implementation. The first step is to present the model on top of which the optimization is performed. In essence, the EMD-TDDFT model consists of coupling a classical system of particles with a quantum many-electron system, and using TDDFT in order to handle the latter.

The classical system is defined by a set of K nuclear coordinates and momenta, $\{R, P\} \equiv \{\vec{R}_\alpha, \vec{P}_\alpha\}_{\alpha=1}^{K}$, where α runs over all the K nuclei, each with mass M_α and charge z_α (atomic units will be used through this article). Their dynamics is coupled to that of a quantum system of N electrons, described by a many-body wave function $\Psi(\vec{r}_1\sigma_1, \ldots, \vec{r}_N\sigma_N)$, where $\vec{r}_n$ and σ_n represent the orbital and spin degrees of freedom of one electron ($\sigma_n = \uparrow, \downarrow$). The EMD model

is then given by the following equations of motion:

$$\dot{\vec{R}}_\alpha(t) = \frac{1}{M_\alpha}\vec{P}_\alpha(t)\,, \tag{1}$$

$$\dot{\vec{P}}_\alpha(t) = \vec{F}_\alpha[R(t),\Psi(t),u,t]\,, \tag{2}$$

$$|\dot{\Psi}(t)\rangle = -\mathrm{i}\hat{H}[R(t),u,t]|\Psi(t)\rangle \tag{3}$$

In these equations, the force $\vec{F}_\alpha[R(t),\Psi(t),u,t]$ is:

$$\vec{F}_\alpha[R(t),\Psi(t),u,t] = -\vec{\nabla}_\alpha W^{\mathrm{nn}}(R(t)) + z_\alpha\varepsilon(u,t)\vec{\pi} - \langle\Psi(t)|\nabla_\alpha\hat{H}[R(t),u,t]|\Psi(t)\rangle\,, \tag{4}$$

The nucleus-nucleus interaction function has the usual Coulomb form:

$$W(R) = \sum_{\beta<\gamma}\frac{z_\beta z_\gamma}{|\vec{R}_\beta - \vec{R}_\gamma|}\,. \tag{5}$$

The time-dependent function $\epsilon(u,t)$ is the amplitude of the electric field of the laser pulse (I ignore the magnetic component, and assume the dipole approximation and the length gauge). The light is polarized in the direction given by the unit vector $\vec{\pi}$. The symbol u represents a set of parameters $u_1, u_2, \ldots, u_M$ that are the ones that can be *controlled*, determining the precise shape of the laser pulse.

Finally, the dynamics of the electrons is determined by the following Hamiltonian:

$$\hat{H}[R,u,t] = \sum_{i=1}^{N}\frac{\hat{\vec{p}}_i^{\,2}}{2} + \sum_{i<j}\frac{1}{|\hat{\vec{r}}_i - \hat{\vec{r}}_j|} + \varepsilon(u,t)\sum_{i=1}^{n}\hat{\vec{r}}_i\cdot\vec{\pi} + \sum_{i=1}^{N}\sum_{\beta}v^\beta(|\hat{\vec{r}}_i - \vec{R}_\beta(t)|)\,. \tag{6}$$

The position and momenta operators of the N electrons are $\hat{\vec{r}}_i$ and $\hat{\vec{p}}_i$, respectively. Note the presence of the electron-nucleus interaction, the last term of the Hamiltonian, which typically is given by (local) Coulomb terms:

$$v^\beta(r) = -\frac{z_\beta}{r}\,. \tag{7}$$

However, sometimes the electron-nucleus interaction is handled with the help of pseudo-potentials [25], which may be non-local operators.

The previous equations are those of the EMD model with the true many-electron wave function Ψ. Given the difficulties of manipulating such a large object, the TDDFT Kohn-Sham (KS) formalism substitutes the real electronic system by a fictitious non-interacting set of electrons, that can be described by a single Slater determinant characterized by N spin orbitals $\varphi_1, \ldots, \varphi_N$. The time-dependent one-electron density of both systems are, however, identical by construction. The spin-resolved version of this density is defined, for the true many-electron wave function Ψ, as:

$$n_{\sigma\tau}(\vec{r},t) = \langle\Psi(t)|\hat{\psi}^\dagger_\sigma(\vec{r})\hat{\psi}_\tau(\vec{r})|\Psi(t)\rangle\,, \tag{8}$$

using the creation and annihilation field operators $\hat{\psi}^\dagger_\sigma(\vec{r})$ and $\hat{\psi}_\tau(\vec{r})$, respectively. The Kohn-Sham spin orbitals, however, permit an easier computation of this object, as:

$$n_{\sigma\tau}(\vec{r},t) = \sum_{m=1}^{N} \varphi^*_m(\vec{r}\sigma,t)\varphi_m(\vec{r}\tau,t)\,. \tag{9}$$

In many situations, the problem does not affect the spin degrees of freedom (i.e. there are no magnetic fields, and the spin-orbit coupling term can be ignored), and the number of electrons is even, which allows for a *spin-restricted* treatment: the Kohn-Sham spin-orbitals φ_m can be grouped in pairs that share the same orbital shape, but have opposite spin quantum number. In the following we will assume this restriction in order to simplify the notation, since the numerical examples shown below fall into this category. The time-dependent density is then:

$$n_t(\vec{r}) \equiv n(\vec{r},t) = \sum_{m=1}^{N/2} 2|\varphi_m(\vec{r},t)|^2\,. \tag{10}$$

The dynamics of the KS orbitals is governed by the time-dependent KS equations, a set of non-linear Schrödinger-like equations:

$$\mathrm{i}\frac{\mathrm{d}}{\mathrm{d}t}|\varphi_i(t)\rangle = \hat{H}_{\mathrm{KS}}[R(t),n_t,u,t]|\varphi_i(t)\rangle \quad (i=1,\ldots,N/2)\,, \tag{11}$$

The Kohn-Sham Hamiltonian $\hat{H}_{\mathrm{KS}}$ is defined as:

$$\begin{aligned}\hat{H}_{\mathrm{KS}}[R(t),n_t,u,t] &= \frac{1}{2}\hat{\vec{p}}^2 + \sum_\beta \hat{v}^\beta(|\hat{\vec{r}}-\vec{R}_\beta(t)|) + \varepsilon(u,t)\hat{\vec{r}}\cdot\vec{\pi} \\ &\quad + \int \mathrm{d}^3r'\,\frac{n_t(\vec{r}')}{|\vec{r}-\vec{r}'|} + v_{\mathrm{xc}}[n_t](\vec{r})\,.\end{aligned} \tag{12}$$

The next-to-last term is the Hartree potential, whereas the last term is the exchange and correlation potential, whose exact form is unknown and must be approximated. We assume an *adiabatic* approximation, meaning that it depends at each time t on the density at that time only, n_t. In particular, we will simply use the adiabatic local density approximation (ALDA).

The EMD-TDDFT model is then determined by the KS equations (Eqs. 11), plus the equations for the classical degrees of freedom, Eqs. 1 and 2, although the force is not any more a functional of the many-electron wave function Ψ, but has the following form that depends on the Kohn-Sham orbitals $\varphi \equiv \{\varphi_m\}_{m=1}^{N/2}$:

$$\begin{aligned}\vec{F}_\alpha[R(t),\varphi(t),u,t] &= -\vec{\nabla}_\alpha W^{\mathrm{nn}}(R(t)) + z_\alpha\varepsilon(u,t)\vec{\pi} \\ &\quad - \sum_{m=1}^{N/2} 2\langle\varphi_m(t)|\,\vec{\nabla}_\alpha v^\alpha(|\hat{\vec{r}}-\vec{R}_\alpha(t)|)\,|\varphi_m(t)\rangle\,.\end{aligned} \tag{13}$$

Once the model that describes the dynamics of the system is completely specified, the objective is to search in the parameter space u those values that

optimize the behavior of the system with respect to a physical goal, e.g. the cleavage of a chemical bond, the ionization of the system, or the population of some electronic excited state. This can be formulated as the maximization of a target functional that depends on the system variables, i.e.:

$$\mathcal{F} = \mathcal{F}[n_T, R(T), P(T), u]\,. \tag{14}$$

The time T is the final time of the propagation interval $[0, T]$ (it is also possible to formulate OCT for a target functional that depends on the evolution of the system during the full interval, and not only on its final state). Note the dependence on the control parameters u, which may be used to favor or penalize regions of the parameter space. However, in the example below the target functional will only depend on the classical variables, i.e. $\mathcal{F} = \mathcal{F}[R(T), P(T)]$, and therefore that restriction will be assumed hereafter (the general formulation can be found in Ref. [22].

The specification of a set of parameters u determines the evolution of the system:

$$u \to R[u], P[u], \varphi[u] \tag{15}$$

In consequence, the problem is reduced to that of maximizing a function:

$$G[u] = \mathcal{F}[R[u](T), P[u](T)]\,. \tag{16}$$

The tools of OCT permit then to obtain an expression for the gradient of G (see Eqs. (30) and (31) in Ref. [22]):

$$\frac{\partial G}{\partial u_k}(u) = \int_0^T \mathrm{d}t\ \frac{\partial \varepsilon}{\partial u_k}(u,t) g(t)\,, \tag{17}$$

where g is:

$$g(t) = -\sum_\beta z_\beta \tilde{\vec{R}}_\beta(t) \cdot \vec{\pi} + 2\mathrm{Im} \sum_{m=1}^{N/2} \langle \chi_m(t) | \hat{\vec{r}} \cdot \vec{\pi} | \varphi_m(t) \rangle\,. \tag{18}$$

Note the appearance of new objects: new position and momenta variables $\tilde{\vec{R}}_\beta, \tilde{\vec{P}}_\beta$ and one-particle orbitals, $\{\chi_m\}_{m=1}^{N/2}$; together they form a *costate*, an auxiliary quantum-classical system whose evolution must be computed in order to obtain

g; the equations of motion for the costate are:

$$\dot{\tilde{\vec{R}}}_\alpha(t) = \frac{1}{M_\alpha}\tilde{\vec{P}}_\alpha(t)\,, \tag{19}$$

$$\begin{aligned}\dot{\tilde{\vec{P}}}_\alpha(t) &= \vec{\nabla}_\alpha\{\sum_\beta \tilde{\vec{R}}_\beta(t)\cdot\vec{F}_\beta[R(t),\varphi(t),u,t]\} \\ &\quad +2\mathrm{Re}\,\mathrm{i}\sum_{m=1}^{N/2}\langle\chi_m(t)|\vec{\nabla}_\alpha\hat{H}_{\mathrm{KS}}[R(t),n_t,u,t]|\varphi_m\rangle\,,\end{aligned} \tag{20}$$

$$\begin{aligned}|\dot{\chi}_m(t)\rangle &= -\mathrm{i}\hat{H}_{\mathrm{KS}}[R(t),u,t]|\chi_m(t)\rangle\,, \\ &\quad -\mathrm{i}\sum_{n=1}^{N/2}\hat{K}_{mn}[\varphi(t)]|\chi_n(t)\rangle \\ &\quad -2\sum_\beta\tilde{\vec{R}}_\beta\cdot\vec{\nabla}_\beta\hat{v}^\beta(|\hat{\vec{r}}-\vec{R}_\beta(t)|)|\varphi_m(t)\rangle\end{aligned} \tag{21}$$

The equations for the evolution of the costate orbitals χ_m contain a new, non-Hermitian term:

$$\langle\vec{r}|\hat{K}_{mn}[\varphi(t)]|\chi_m(t)\rangle = -4\mathrm{i}\varphi_m(\vec{r},t)\mathrm{Im}\int\mathrm{d}^3r'\chi_n(\vec{r},t)f_{\mathrm{Hxc}}[n_t](\vec{r},\vec{r}')\varphi_n(\vec{r},t)\,, \tag{22}$$

where $f_{\mathrm{Hxc}}[n_t](\vec{r},\vec{r}')$ is the "kernel" of the KS Hamiltonian, defined as the functional derivative of that Hamiltonian with respect to the density:

$$f_{\mathrm{Hxc}}[n](\vec{r},\vec{r}') = \frac{1}{|\vec{r}-\vec{r}'|} + \frac{\delta v_{\mathrm{xc}}[n](\vec{r})}{\delta n(\vec{r}')}\,. \tag{23}$$

These expressions assume an adiabatic approximation for the exchange and correlation potential v_{xc}, i.e. its functional dependence on the density is only through its instantaneous value at a given time, and not on it full history, as the exact theory prescribes. A non-adiabatic functional would lead to a more complicated Eq. 22: the space integral in the right hand side would also be a time integral. This would complicate the numerical integration of the costate evolution, in a similar way that the non-adiabatic approximation would complicate the normal Kohn-Sham states evolution. In the examples below, we have used the ALDA. The use of better – yet still adiabatic – approximations does not significantly complicate the numerics, unless the computation of the kernel in Eq. 23 is itself complicated.

The equations of motion for the costate must be supplemented by the corresponding boundary conditions, which are:

$$\tilde{\vec{R}}_\alpha(T) = -\frac{\partial}{\partial\vec{P}_\alpha}\mathcal{F}(R(T),P(T))\,, \tag{24}$$

$$\tilde{\vec{P}}_\alpha(T) = \frac{\partial}{\partial\vec{R}_\alpha}\mathcal{F}(R(T),P(T))\,, \tag{25}$$

$$|\chi_m(T)\rangle = 0\,. \tag{26}$$

These are not *initial* value conditions, but *final* value conditions. Therefore, the computation of the gradient components of G must be performed as follows: first, propagate *forwards* the equations of motion for the system state (Eqs. 1, 2 and 11), a propagation that also permits to compute the value of the function, $G(u)$. Then, propagate *backwards* the equations of motion of the costate (Eqs. 19, 20 and 21), starting from the final value conditions 24, 25, and 26.

Once there is a procedure to compute $G(u)$ and $\nabla G(u)$, the next step is choosing an optimization algorithm. In the examples shown below, the Broyden-Fletcher-Goldfarb-Shanno quasi-Newton algorithm (BFGS) [26] as implemented in the GSL mathematical library [27].

Before moving on to the description of some examples of application, I will describe the salient features of the numerical implementation of these equations, which has been done on top of the octopus code [23, 24]. This code specializes in the solution of the TDDFT equations for a wide variety of systems. Its most relevant numerical characteristics are:

- It is mostly a *real-space* code: the wave functions, densities, potentials, etc. are represented by the values that they take on a regular mesh of points in real space. In this representation, the potential operator are in principle local (i.e. diagonal; but see the next point about pseudo-potentials), whereas the kinetic operator is a non-local finite-difference expression, i.e. it is computed through a very sparse matrix-vector operation.

- The electron-ion interaction is handled with the help of pseudo-potentials [25], which both avoids the Coulomb discontinuity at zero electron-nucleus distance, and permits to avoid the explicit treatment of the inert core-electrons. However, they are non-linear operators in real space.

- The time-propagation can be handled with a variety of algorithms [28]. For this work, I have used the 4th order explicit Runge-Kutta scheme (RK4) [29, 30]. The propagation error is fourth-error in the time-step. If the computation of the integral in Eq. 17 is also performed with a fourth order scheme, the overall error in the calculation of the gradient is also of order four.

- The control parameters u that define the precise shape of the electric field amplitude $\varepsilon(u,t)$ are defined as in Ref. [21]: First, the pulse temporal shape is expanded in a Fourier series:

$$\varepsilon(t) = \sum_{i=1}^{2L} \varepsilon_i(u) g_i(t)\,, \tag{27}$$

where

$$g_i(t) = \begin{cases} \sqrt{\frac{2}{T}} \cos\left(\frac{2\pi}{T} i t\right) & (i = 1, \ldots, L) \\ \sqrt{\frac{2}{T}} \sin\left(\frac{2\pi}{T} (i-L) t\right) & (i = L+1, \ldots, 2L) \end{cases} \tag{28}$$

This fixes a maximum possible (*cut-off*) frequency to $\frac{2\pi}{T}L$. Note the zero-frequency term is explicitly omitted, which is a desired restriction, in order to fulfill the physical condition

$$\int_0^T \mathrm{d}t\ \varepsilon(t) = 0\,. \tag{29}$$

The coefficients ε_i are not, however, directly identical to the optimization parameters $u_1, \ldots, u_M \equiv u$, but are function of them. The reason is that there are other conditions that are enforced: First, the preservation of the *fluence*, or integrated intensity over the duration of the pulse, defined as:

$$F(u) = \int_0^T \mathrm{d}t\ \varepsilon^2(u,t)\,. \tag{30}$$

The search is performed only in the set of pulses whose fluence equals a given value F_0 (a fully unconstrained search would in this case lead to a problem without an optimum, since it would allow pulses with unlimited intensities). Second, other obvious conditions that must be fulfilled are:

$$\varepsilon(u,0) = \varepsilon(u,T) = 0\,. \tag{31}$$

The parameters u are chosen to fulfill all these conditions, as described in Ref. [21].

In the calculations below, the total propagation time T is set to ≈ 157.a.u. ≈ 3.8 fs, which amounts to 25ω cycles of frequency $\omega = 1$ a.u. The cut-off is set at 2 a.u. This means 100 Fourier coefficients, which implies 98 degrees of freedom due to the constraints described above.

4 Examples of application

4.1 Hydrogen molecule

The optimal dissociation of the Hydrogen with the QOCT-TDDFT methodology molecule was studied in Ref. [21]. The goal now is to prove that the problems encountered then, due to the use of an optimization scheme that ignored nuclear movement, can be solved with the full quantum-classical optimal control presented in Ref. [22]. Let us recall the key points of that attempt: the definition of the target was:

$$\mathcal{F}[n] = P_{1x}[n_T] - P_{2x}[n_T]\,, \tag{32}$$

where

$$\vec{P}_\alpha[n] = \int_0^T \mathrm{d}t \vec{F}_\alpha[n_t] = -\int_0^T \mathrm{d}t \int \mathrm{d}^3 r\ n(\vec{r},t)\vec{\nabla}_\alpha v_0(\vec{r};\underline{R})\,. \tag{33}$$

is the time-integrated force on each nucleus. In that calculation, the nuclei were not allowed to move during the optimization runs, under the assumption that

the pulse is short enough to ignore that movement. However, the system would "accumulate momentum" through the excitation of the electronic system, leading to dissociation after the pulse has ended. For the laser pulse length chosen ($\approx$ 157.a.u.), this proved to be sufficient when the laser fluence was sufficiently high, but not for lower fluences. In that case, the neglect of the ionic movement in the optimization caused the optimal pulse to perform badly at its task of accelerating the nuclei away from each other when the pulse was used with moving nuclei. This can be seen in the lower panels of Fig. 1, which are the calculations presented in Ref. [21], repeated here for convenience. These calculations are Ehrenfest propagations (i.e. nuclei are allowed to move) performed with the optimal pulse.

In the bottom-left panel, one can see the internuclear distance as a function of time, which first increases, but is then reduced, showing how the system does not dissociate, but would stay oscillating around the equilibrium configuration. The reason for the failure can be learnt from the bottom-right panel, which shows the relative force on the nuclei: it increases during the first half of the laser pulse (the shadowed area in the plots), but does not reach a very high value, and moreover it diminishes during the second half of the laser pulse. The optimal pulse was designed by the optimization procedure to increase the forces acting on the *static* nuclei, but does not perform so well on the forces acting on the moving nuclei.

The new optimization procedure described above should account for the nuclear movement, and solve the problem. The target functional used now is:

$$\mathcal{F}[R(t), P(t)] = (\vec{P}_1(T) - \vec{P}_2(T))^2 \,, \tag{34}$$

i.e. the two Hydrogen atoms should have the largest possible relative momenta at the final time of the pulse. This choice of target is similar to the one used in Ref. [21], and it amounts to maximizing the average relative force during the action of the pulse. Afterwards, the gained dissociative momentum should be enough to separate the atoms definitively.

The numerical parameters and settings were equal to those used in Ref. [21]. The (initial) bond-length is 1.44 a.u. The nucleus-electron interaction is not Coulombic, but softened through the pseudo-potential method [25]. This is necessary to avoid singularities in the calculation, since all functions (wave functions, potentials, etc.) are represented on a real-space regular cubic mesh. The grid spacing is chosen to be 0.4 a.u., and the simulation box used during the optimization is a sphere of radius 13 a.u. However, the performance of the final optimal pulses are checked with a simulation box twice as large, in order to make sure the calculations are converged with respect to box size. Regarding the computational cost, each forward propagation requires 30 minutes when performed on four cores of an AMD Opteron 6376 processor, whereas the backward propagations are twice as long, approximately. The optimization algorithm is completed after around 100 function and function-gradient evaluations – these numbers depend on the number of degrees of freedom of the laser pulse search space, the initial guess, etc.

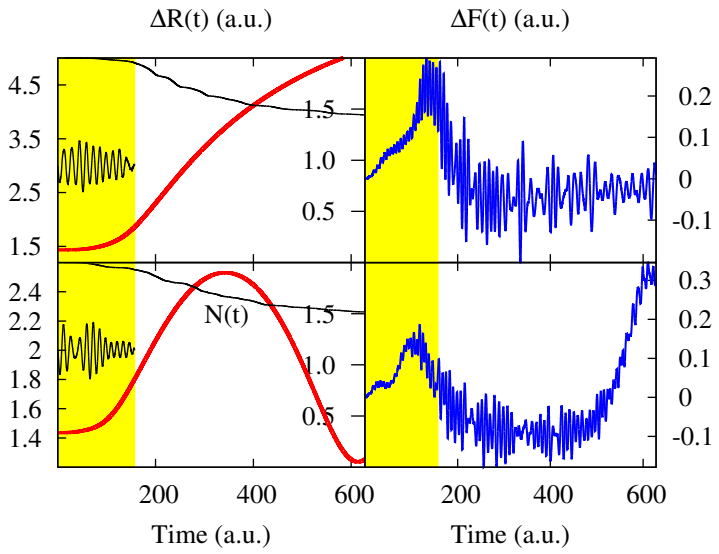

Figure 1: Internuclear distance (left panels) and relative forces (right panels) of the nuclei of the Hydrogen molecule, for the pulse obtained performed with the fixed-nuclei optimization scheme (bottom), and for the pulse obtained with then new QOCT for the Ehrenfest model (top). In the left panels, the total charge $N(t)$ contained in the simulation region is also overlaid (thin lines, scale of the y-axis on the right side of each plot). The shadowed region marks the time during which the pulse acts on the system; the pulses are also drawn, in arbitrary units, on the left panels.

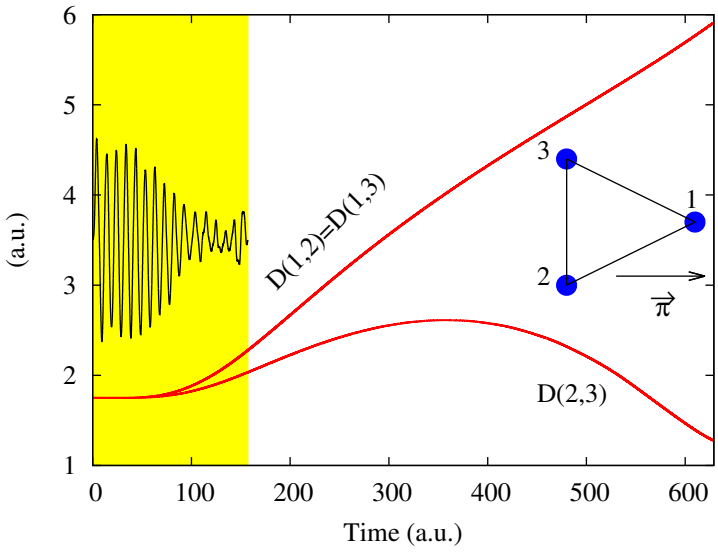

Figure 2: Distances among the nuclei of the H_3^+ cation, when irradiated with the optimal pulse obtained by the maximization algorithm. The shadowed region marks the time during which the pulse acts on the system; the pulse is also represented in this shadowed area, in arbitrary units. The vector $\vec{\pi}$ marks the pulse polarization with respect to the nuclear positions, labeled 1, 2 and 3 in the diagram. Notice that the distances D(1,2) and D(1,3) are equal due to symmetry.

The initial guess for the new optimization is the optimal pulse obtained previously and reported in Ref. [21]. Then, the algorithm searches for better-performing pulses in the search space described above: pulses with equal fluence, with a maximum cut-off of 2 a.u. The Ehrenfest simulation performed with the new optimum is shown in Fig. 1, top panels. The system clearly dissociates, and the reason can be understood by looking at the internuclear forces (top right panel), compared to the ones that were obtained with the previous optimal pulse (top left panel): the forces are larger, and they keep increasing until almost the end of the pulse action. The pulses, both the initial guess – which was the optimal one in Ref. [21] – and the new optimum, are also drawn in Fig. 1, above the grey-shaded are that represents the first $\approx$ 157 a.u. of simulation. Their average intensities are $\approx 3 \times 10^{12}$ W/cm^2.

4.2 Trihydrogen cation

The second example is the H_3^+ cation. We approached this problem previously [20], where we used a gradient-free optimization algorithm, on top of the EMD-TDDFT model. Gradient-free algorithms allow to by-pass the backward-

propagation equations of QOCT, but are not as efficient as the algorithms that use the gradient. Now, I have approached the same problem, using the full QOCT for the EMD-TDDFT model described above. The goal is to obtain a selective photo-dissociation, breaking the molecule in a prescribed way. In this case, there are three identical bonds, and therefore it is specially challenging to address some of the bonds specifically. The laser pulse should take out one of the Hydrogen atoms, leaving behind a bound Hydrogen molecule. The chosen Hydrogen atom is number 1 in the notation of the inset of Fig. 2.

The definition of the target follows the pattern used in the previous example:

$$\mathcal{F}[R(t), P(t)] = (\vec{P}_1(T) - \vec{P}_2(T))^2 + (\vec{P}_1(T) - \vec{P}_3(T))^2 - (\vec{P}_2(T) - \vec{P}_3(T))^2 \,. \quad (35)$$

The meaning of this definition is the following: at the end of the pulse, the relative momenta between the nuclei that need to be separated should be as large as possible (hence the positive sign of the first two terms), whereas the relative momenta between the nuclei that need to stay bound should be small (hence the negative sign of the last one).

The laser pulse length was chosen to be equal to the one used for the H2 case ($\approx 157 a.u.$). This is substantially shorter than the 400 a.u. used in Ref. [20]; we will see how the new methodology is able to find a successful pulse even in this very fast time scale. The search space, spanning 98 degrees of freedom, is also the same. The cost of these calculations was similar to the cost of the calculations of the Hydrogen molecule. The results obtained with the optimal pulse found by the algorithm are shown in Fig. 2. It can be seen how the the distances between nuclei 1 and 3 and 1 and 2 rapidly grow, leading to the dissociation of atom 1, whereas nuclei 2 and three remain bound – although in a highly excited vibrational state.

Finally, Fig. 3 displays the power spectra of the optimal pulses, both for the Hydrogen molecule case (bottom), and for the H_3^+ case (top). They are shown together with the photo-absorption cross section of both systems, computed with the real-time propagation TDDFT technique [31], assuming the laser polarization orientation used in the OCT calculations. This permits to compare the spectral decomposition of the pulses with the key excitations of both the Hydrogen molecule and of the trihydrogen cation, as predicted by TDDFT with the ALDA, since these are located at the peaks of the photo-absorption cross section. It is clear that, unsurprisingly, the optimization algorithm creates pulses whose power spectrum is centered around the main resonances, in order to maximize the system response. However, there are other important minor components: simple quasi-monochromatic pulses tuned to the main references would not induce the same reaction.

It is also noteworthy the difference, for the Hydrogen molecule case, between the pulse optimized with the fixed-nucleus approximation in Ref. [22] (green in Fig. 3), and the new optimal pulse. The strong difference stresses, once more, the necessity of using a combined electron-ion dynamics scheme in combination with OCT.

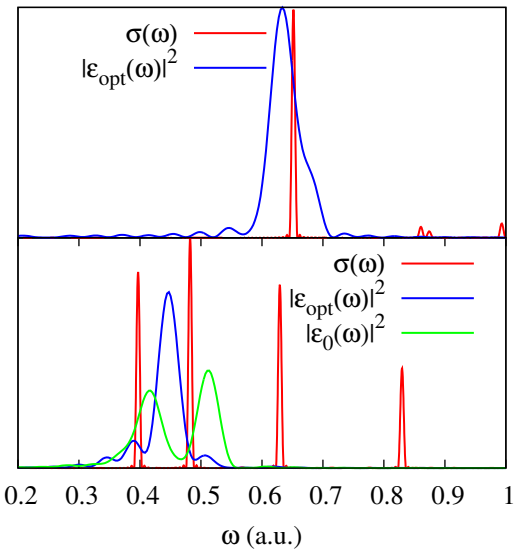

Figure 3: Photo-absorption cross section ($\sigma(\omega)$) and power spectrum of the optimal pulses ($|\varepsilon_{\rm opt}(\omega)|^2$) for the Hydrogen molecule (bottom) and the trihydrogen cation (top). For the former, the initial guess pulse ($|\varepsilon_0(\omega)|^2$) is also shown (this initial pulse is in fact the optimal pulse obtained in the fixed-pulse approximation approach reported in Ref. [22]). All plots are shown in arbitrary units.

5 Conclusions

An optimal control theory can be worked out for the EMD-TDDFT molecular dynamics scheme; in this article I have reported its numerical implementation and some first examples of application. The work essentially consists of enhancing the combination of TDDFT and QOCT reported in Ref. [19], to deal with systems containing both electrons and nuclei, described with the EMD-TDDFT formalism. It is the first application of optimal control to a molecular dynamics model.

The method has been used to obtain ultra-fast photo-dissociation for the Hydrogen molecule and the H_3^+ cation. This goal is achieved by maximizing a target functional constructed by considering the momenta of the nuclei at the end of the propagation time: the relative momenta of the nuclei that one wants to break apart are to be maximized, whereas in order for the dissociation to be "selective", one also wants to make the relative momenta of the nuclei that one wants to keep bound small.

The equations that result are numerically tractable, and the good scalability of TDDFT permits to foresee the extension of this work, that has only considered two-electron very small molecules, to larger systems. The work in this direction is in progress. The biggest challenge is, however, the reliability of current approximations to the exchange-and-correlation functional in TDDFT. Any application of TDDFT to the non-linear interaction of many-electron systems with light, such as the one proposed here, is subject to the error of these approximations. It is to be expected that these will improve in the coming years. This first demonstration of use of optimal control for a non-adiabatic molecular dynamics scheme opens the way to other possibilities – dynamics based on other quantum chemistry approaches, or on other quantum/classical coupling schemes, such as surface hopping, etc.

6 Acknowledgment

I acknowledge financial support from the Spanish MINECO grant FIS2013-46159-C3-1-P.

7 Keywords

Time-dependent density-functional theory, optimal control theory, attosecond physics, photo-dissociation.

References

[1] Constantin Brif, Raj Chakrabarti, and Herschel Rabitz. Control of quantum phenomena: past, present and future. *New Journal of Physics*, 12(7):075008, July 2010.

[2] M. Shapiro and P. Brumer. *Principles of the Quantum Control of Molecular Processes*. Wiley, New York, 2003.

[3] S. A. Rice and M. Zhao. *Optical Control of Molecular Dynamics*. John Wiley & Sons, New York, 2000.

[4] A. Assion, T. Baumert, M. Bergt, T. Brixner, B. Kiefer, V. Seyfried, M. Strehle, and G. Gerber. Control of chemical reactions by feedback-optimized phase-shaped femtosecond laser pulses. *Science*, 282(5390):919–922, 1998.

[5] Robert J. Levis, Getahun M. Menkir, and Herschel Rabitz. Selective Bond Dissociation and Rearrangement with Optimally Tailored, Strong-Field Laser Pulses. *Science*, 292:709–713, 2001.

[6] T. Laarmann, I. Shchatsinin, P. Singh, M. Zhavoronkov, M. Gerhards, C. P. Schulz, and I. V. Hertel. Coherent control of bond breaking in amino acid complexes with tailored femtosecond pulses. *Journal of Chemical Physics*, 127:201101, 2007.

[7] RS Judson and Herschel Rabitz. Teaching lasers to control molecules. *Physical Review Letters*, 68(10):1500, 1992.

[8] A. M. Weiner. Femtosecond pulse shaping using spatial light modulators. *Review of Scientific Instruments*, 71(5):1929, 2000.

[9] David G. Luenberger. *Optimization by vector space methods*. John Wiley & Sons, Inc., New York, 1969.

[10] E Runge and EKU Gross. Density-functional theory for time-dependent systems. *Physical Review Letters*, 52:997–1000, 1984.

[11] M. A. L. Marques, C. A. Ullrich, F. Nogueira, A. Rubio, K Burke, and E. K. U. Gross, editors. *Time-Dependent Density Functional Theory*. Springer Verlag, Berlin, 2006.

[12] U Saalmann and R Schmidt. Non-adiabatic quantum molecular dynamics: basic formalism and case study. *Zeitschrift für Physik D Atoms, Molecules and ...*, 38:153–163, 1996.

[13] F Calvayrac, P.-G Reinhard, and E Suraud. Coulomb explosion of an cluster in a diabatic electron-ion dynamical picture. *Journal of Physics B: Atomic, Molecular and Optical Physics*, 31:5023–5030, 1998.

[14] U Saalmann and R Schmidt. Excitation and relaxation in atom-cluster collisions. *Physical Review Letters*, 80:3213–3216, 1998.

[15] Thomas Kunert and Rüdiger Schmidt. Excitation and fragmentation mechanisms in ion-fullerene collisions. *Physical review letters*, 86:5258, 2001.

[16] A Castro, MAL Marques, JA Alonso, GF Bertsch, and A Rubio. Excited states dynamics in time-dependent density functional theory: high-field molecular dissociation and harmonic generation. *European Physical Journal D*, 28:211–218, 2004.

[17] Thomas Kunert, Frank Grossmann, and Rüdiger Schmidt. Nonadiabatic dynamics of ethylene in femtosecond laser pulses. *Physical review. A*, 72:023422, 2005.

[18] A Castro, M Isla, JI Martínez, and JA Alonso. Scattering of a proton with the Li 4 cluster: Non-adiabatic molecular dynamics description based on time-dependent density-functional theory. *Chemical Physics*, 399:130–134, 2012.

[19] A Castro, J Werschnik, and EKU Gross. Controlling the Dynamics of Many-Electron Systems from First Principles: A Combination of Optimal Control and Time-Dependent Density-Functional Theory. *Physical Review Letters*, 109:153603, 2012.

[20] Kevin Krieger, Alberto Castro, and EKU Gross. Optimization schemes for selective molecular cleavage with tailored ultrashort laser pulses. *Chemical Physics*, 391:50–61, 2011.

[21] A Castro. Theoretical Shaping of Femtosecond Laser Pulses for Ultrafast Molecular Photodissociation with Control Techniques Based on Time Dependent Density Functional Theory. *ChemPhysChem*, 14:1488–1495, 2013.

[22] A Castro and E. K. U. Gross. Optimal control theory for quantum-classical systems: Ehrenfest molecular dynamics based on time-dependent density-functional theory. *Journal of Physics A: Mathematical and Theoretical*, 47(2):025204, January 2014.

[23] A Castro, H Appel, M Oliveira, C A Rozzi, X Andrade, F Lorenzen, M. A. L. Marques, E. K. U. Gross, and A Rubio. octopus: a tool for the application of timedependent density functional theory. *Physica Status Solidi (b)*, 243:2465–2488, 2006.

[24] Miguel A L Marques, Alberto Castro, George F Bertsch, and Angel Rubio. octopus: a first-principles tool for excited electron-ion dynamics. *Computer Physics Communications*, 151:60–78, 2003.

[25] N. Troullier and JL Martins. Efficient pseudopotentials for plane-wave calculations. *Physical Review B*, 43(3):1993, 1991.

[26] R. Fletcher. *Practical Methods of Optimization*. Wiley, New York, 2000.

[27] M. Galassi, J. Davies, J. Theiler, B. Gough, G. Jungman, P. Alken, M. Booth, and F. Rossi. *GNU Scientific Library*. Network Theory Limited, 2009.

[28] Alberto Castro, MAL Marques, and Angel Rubio. Propagators for the time-dependent KohnSham equations. *The Journal of chemical physics*, 121(8), 2004.

[29] C. Runge. Über die numerische auflösung von differentialgleichungen. *Math. Ann.*, 46:167–178, 1895.

[30] W. Kutta. Beitrag zur naherungsweisen integration von differentialgleichungen. *Z. Math. und Phys.*, 46:435–453, 1901.

[31] K. Yabana and G. F. Bertsch. Time-dependent local-density approximation in real time. *Physical Review B*, 54(7):4484–4487, 1996.